Controlling Eu^{2+} Substitution towards a Narrow-Band Green-Emitting Borate Phosphor $NaBaB_9O_{15}:Eu^{2+}$

Ya Zhuo, Jiyou Zhong, Jakoah Brgoch*

Department of Chemistry, University of Houston, Houston, TX 77204, USA

*Corresponding author. Email: jbrgoch@uh.edu

Abstract

Highly efficient, thermally stable, narrow-band phosphors that can be excited by a blue LED chip are crucial for energy-efficient light bulbs and display lighting. Here, a rare narrow-band, green-emitting phosphor based on the compound $NaBaB_9O_{15}:Eu^{2+}$ is demonstrated. The emission peak is centered at 515 nm with a full-width at half-maximum (fwhm) of 61 nm (2294 cm^{-1}), and a photoluminescence quantum yield of >80% using blue or near-UV LED excitation. This borate's remarkable green emission stems from Eu^{2+} substituting on the smaller [NaO_6] polyhedron instead of the larger and more favorable [BaO_9] polyhedron. The phosphor also exhibits negligible thermal quenching up to 650 K owing to the wide band gap, high connectivity of the rigid $NaBaB_9O_{15}$ crystal structure, and the depopulation of trap-states. This combination of optical properties and its straightforward synthesis conditions makes $NaBaB_9O_{15}:Eu^{2+}$ an ideal green phosphor for next-generation LED-based lighting or display systems.

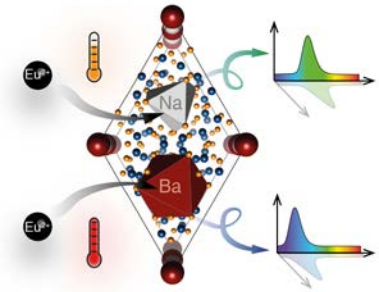

Introduction

Phosphor-converted white light emitting diodes (pc-LED) are the most promising lighting source for next-generation backlighting display applications as well as general white lighting owing to their high efficiency, long lifespan, low energy consumption, and environmentally benign chemical composition.[1,2] These devices operate by converting the nearly monochromatic emission from a LED chip using one, or more, rare-earth substituted inorganic phosphors.[3–5] The most common inorganic phosphors, in the case of backlighting, for example, include the green-emitting β-SiAlON:Eu^{2+}, which has the emission centered at 540 nm with a full width at half maximum (fwhm) of 55 nm and the red-emitting phosphor $K_2SiF_6:Mn^{4+}$, which has a sharp emission at 630 nm.[6,7] This combination of luminescent materials and a blue LED chip covers a majority of the color gamut, as determined by the color coordinates of the red, green, and blue (RGB) emission; yet, there is ample room to expand the color gamut by switching to narrow-band phosphors. Indeed, recent research by groups around the world has yielded a plethora of new and improved red and blue-emitting phosphors.[8–11] Even with the success of these materials, there remains a significant lack of new green phosphors discovered. Considering the human eye is sensitive to the green

spectral region most, there is an outstanding need to identify new highly efficient, narrow green-emitting phosphors.

There are only a few green phosphors known that fulfill the stringent requirements for application, which include a narrow emission band with an appropriate peak position, a high efficiency, and excellent thermal stability. For example, β-SiAlON:Eu^{2+} is the narrowest commercial green phosphor, but its emission coordinates limit the maximum accessible color gamut. Additionally, the preparation of this phosphor requires extreme conditions, including high-pressure and high-temperature synthesis.[6,12] In contrast, $(Ba,Sr)_2SiO_4$:Eu^{2+} and $SrGa_2S_4$:Eu^{2+} are simple to prepare and require only high-temperature solid-state reaction under mildly reducing conditions. Nevertheless, the broad emission band of the former and the poor thermal and chemical stability of the later remain a challenge.[13,14] Another green phosphor is $RbLi(Li_3SiO_4)_2$:Eu^{2+}. This compound has high efficiency and a narrow emission band, although its chemical stability must be enhanced for industrial application.[15] Finally, quantum dots (QD) emitters are a potential alternative solution with significant advantages, in particular for display lighting; however, research must continue to address their poor chemical and thermal stability as well as their compositions.[16,17] Clearly, it is a major challenge to obtain application-ready narrow-band green-emitting phosphors, which has propelled researchers to establish new design strategies and investigate unconventional crystal chemistries.

There has recently been a re-focus on borate phosphors with new crystal structures or compositions because of their easy synthesis process, various structures, and excellent chemical and physical stability. At present, the luminescence of nearly all borate phosphors, regardless of substitution with Eu^{2+} or Ce^{3+}, produce a blue emission (420–450 nm) after excitation with a UV source.[18] There are virtually no other examples of borates that have electronic transitions outside of this region. The only exception was the report of $NaBaBO_3$:Ce^{3+}, which was suggested to produce a green emission centered at 505 nm.[19] Indeed, this phase is the only member in $MNBO_3$ (M = Li, Na; N = Ca, Sr, Ba) that emits color other than blue. Further work on this phase failed to reproduce these results and instead yielded a blue emission from the same composition.[20] Using computational modeling, this emission discrepancy was attributed to the rare-earth ion substituting on different crystallographic sites. In the case where Ce^{3+} replaces Ba^{2+} in the crystal structure, a blue emission is expected whereas the green emission is observed when Ce^{3+} is occupying Na^+ position due to the smaller polyhedral volume of the $[NaO_6]$ compared to the $[BaO_9]$ causing stronger crystal field splitting of Ce^{3+} 5*d* orbitals. These results suggest that non-blue borate phosphors may be possible provided the rare-earth ion can be selectively substituted for Na^+. The goal of this research is to establish a method to control the rare-earth ion substitution in inorganic phosphors.

Recently a highly efficient blue-emitting borate phosphor with general formula $Na(Ba_{0.97}Eu_{0.03})B_9O_{15}$ was reported.[21] The crystal structure adopts the non-centrosymmetric trigonal space group *R*3*c* (space group no. 161).[22] As illustrated in Fig. 1A, the structure contains an unusual three-dimensional framework of $[B_3O_7]^{5-}$ subunits made of two $[BO_3]^{3-}$trigonal planar units and one $[BO_4]^{5-}$ tetrahedron that are linked through their vertices. The arrangement of the $[B_3O_7]^{5-}$ units generates large tunnels along the [001] direction that are occupied by Ba^{2+} and Na^+ in an alternating fashion. The Ba^{2+} ions are coordinated in a nine-vertex distorted tri-capped trigonal prism whereas Na^+ sits in a smaller, highly distorted trigonal antiprism formed by six oxygen anions. The original synthesis of this phosphor uses a multi-step solid-state reaction at >750°C with metal oxides and carbonates as starting materials. Under these conditions, Eu^{2+}

replaces Ba^{2+} to generate a narrow blue emission (λ_{em} = 416 nm) using UV excitation (λ_{ex} = 315 nm).[21]

In this work, we successfully produced the green version of $NaBaB_9O_{15}:Eu^{2+}$ by shifting the reaction kinetics to drive the substitution of Eu^{2+} onto the Na^+ centered polyhedral site. Owing to the smaller volume of the [NaO_6] polyhedron compared to the larger [BaO_9] unit, $(Na_{0.97}Eu_{0.03})BaB_9O_{15}$ emits at longer than expected wavelength following the enhanced crystal field splitting of the Eu^{2+} 5d orbitals. This phosphor not only shows a green emission under blue excitation with a high photoluminescence quantum yield (Φ), but the emission peak is also narrow and thermally robust. These optical properties make this novel green phosphor a promising alternative for LED-based lighting or display applications. More importantly, the concept of controlling preferential substitution will provide new opportunities for the discovery of luminescent materials.

Results and Discussion

The preparation of the new $(Na_{0.97}Eu_{0.03})BaB_9O_{15}$ (NBBO:Eu_{Na}), as well as $Na(Ba_{0.97}Eu_{0.03})B_9O_{15}$ (NBBO:Eu_{Ba}) as reference, employs a ceramic synthesis route that starts from combinations of metal oxide or metal carbonate powders, as detailed in the supporting information, at 725 °C for NBBO:Eu_{Na} and 780 °C for NBBO:Eu_{Ba} for 30 hours. According to the synchrotron powder X-ray diffractograms,[23] shown in Fig. 1B and Fig. S1, NBBO:Eu_{Ba} is a single-phase product whereas NBBO:Eu_{Na} is nearly phase pure with a minor impurity that belongs to BaB_8O_{13}. The presence of this slight second phase is due to the relatively low synthetic temperature of the target phase. Fortunately, the presence of $BaB_8O_{13}:Eu^{2+}$ does not impede the ensuing structural or optical characterization.

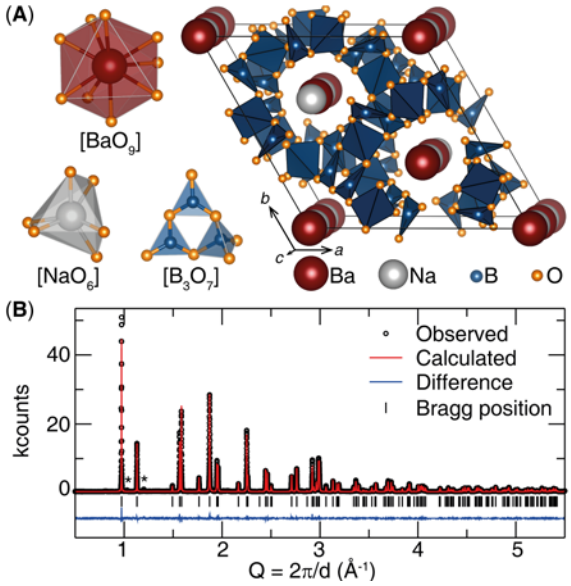

Fig. 1. Structure and Rietveld refinement. (**A**) Crystal structure of $NaBaB_9O_{15}$ with the associated [BaO_9], [NaO_6], and [B_3O_7] polyhedral subunits highlighted. (**B**) Rietveld refinement of $(Na_{0.97}Eu_{0.03})BaB_9O_{15}$ synchrotron X-ray powder diffraction data. Impurity (BaB_8O_{13}) peaks are marked by asterisks.

Considering the ionic radii of the elements present in $NaBaB_9O_{15}$, Eu^{2+} is widely expected to substitute on the Ba^{2+} crystallographic site given that Eu^{2+} ($r_{9\text{-coord.}}$ = 1.30 Å) is smaller than Ba^{2+} ($r_{9\text{-coord.}}$ = 1.47 Å).[24] Indeed, this is observed not only in the original report of $Na(Ba_{0.97}Eu_{0.03})B_9O_{15}$ but many other Ba^{2+} containing phosphors such as $NaBaPO_4:Eu^{2+}$, $BaMgAl_{10}O_{17}:Eu^{2+}$, and $BaAl_2Si_2O_8:Eu^{2+}$.[25–27] However, comparing the ionic radius of 6-coordinate Eu^{2+} ($r_{6\text{-coord}}$ = 1.17 Å) suggests it also be possible for the rare-earth ion to replace Na^+ ($r_{6\text{-coord}}$ = 1.02 Å) because their radius difference is only ≈15%, which is within limits of the Hume-Rothery rules for substitution.[28] Lowering the synthetic temperature to 725 °C, the final product can, in fact, be obtained as desired as metastable state where Eu^{2+} occupies the Na^+ crystallographic site. Eu^{2+} substituting for Na^+ can be proven by comparing the lattice parameters obtained from Rietveld refinements of the synchrotron powder X-ray diffraction data. The refined atom positions and atomic displacement parameters are provided in Table S1 and S2, and the crystallographic data is provided in Table 1. Comparing the refined unit cell volumes shows that taking the unsubstituted NBBO host and substituting Eu^{2+} using a reaction temperature of 780°C causes the unit cell volume to decrease. Given that the rare-earth ionic radius is smaller than the alkaline earth, Eu^{2+} is certainly occupying the Ba^{2+} crystallographic position as anticipated for $NBBO:Eu_{Ba}$. Conversely, employing the lower reaction temperature (725°C) shows the product has a refined lattice parameter that is larger than the unsubstituted NBBO. The only rationalization for this change is that Eu^{2+} must substitute for the smaller Na^+ cation causing the unit cell volume to increase. This substitution preference for Eu^{2+} is certainly metastable because continuing to react the product for a longer time or using a temperature >725 °C results in the rare-earth to occupy Ba^{2+} site.

Further support for the substitution of Eu^{2+} for Na^+ in this phosphor is provided by analyzing the photoluminescence properties. Conducting the reaction at 725°C shows the product has an excitation spectrum that spans from <280 nm to ≈480 nm, as plotted in Fig. 2A. This is critical because it indicates $NBBO:Eu_{Na}$ is a versatile phosphor that can be excited by a variety of LED sources. The emission spectrum (Fig. 2A) when excited using a blue excitation source (λ_{ex} = 430 nm),displays a very narrow emission peak with a maximum centered at 515 nm and a full width at half-maximum (fwhm) of approximately 61 nm (2294 cm^{-1}). The narrow fwhm of this phosphor is comparable to the current narrowest green commercial phosphor, β-SiAlON:Eu^{2+} (fwhm = 55 nm; 1760 cm^{-1}), and it is also narrower than most other green phosphors reported in the literature including the well-known $Ba_2SiO_4:Eu^{2+}$ (fwhm = 80 nm; 2410 cm^{-1}) and $Y_3(Al,Ga)_5O_{12}:Ce^{3+}$ (fwhm = 120 nm; 3750 cm^{-1}).[6,13,29] The $NBBO:Eu_{Na}$ emission spectra measured using typical UV, and near UV excitation sources (λ_{ex} = 330 nm, 365 nm, and 395 nm) all show the same narrow green emission, plotted in Fig. S2. It is worth noting that in some samples, excitation in the UV shows two distinct emission peaks. The main peak is the intense green emission, and there is a minor peak in the blue region, which can be attributed to the small amount of Eu^{2+} substituting on Ba^{2+} site. Optimizing the synthetic conditions should minimize, or eliminate, this peak. The green emission peak can be fit by a single Gaussian curve corresponding to the $5d \rightarrow 4f$ ($^6P_j \rightarrow {}^8S_{7/2}$) electronic transition proving that this luminescence signal stems from the Eu^{2+} occupying the sole crystallographically independent Na^+. The single Eu^{2+} site is further supported by measuring the photoluminescence lifetime, as shown in Fig. S3. The time-gated photoluminescence data were fit using a single exponential function to reveal a luminescence lifetime for the green peak in $NBBO:Eu_{Na}$ of 1.103 μs. This is distinct from the blue emission lifetime in $NBBO:Eu_{Ba}$ of 0.842 μs. These lifetimes are in agreement with the electronic transitions of Eu^{2+} substituted phosphors and are fast enough to minimize any saturation effects allowing these materials to be considered for high-power or potentially laser-based lighting.

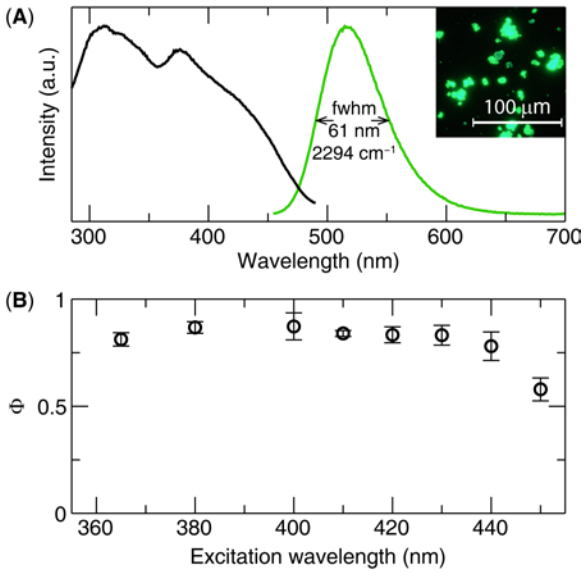

Fig. 2. Luminescence and photoluminescence quantum yield measurements. (**A**) Room temperature excitation spectrum (black) monitored at 515 nm and emission (green) spectrum excited at 430 nm of NBBO:Eu_{Na}. The inset shows a photograph of the bright green emission produced by this phosphor. (**B**) Room temperature photoluminescence quantum yield (Φ) of NBBO:Eu_{Na} determined using different excitation wavelengths.

Although this phosphor has a narrow emission, to be industrially relevant NBBO:Eu_{Na} must also have high efficiency. Therefore, the room temperature photoluminescence quantum yield (Φ) was measured to assess the phosphor's internal efficiency. Because of the broad excitation spectrum, the Φ of the green emission was measured using multiple excitation wavelengths to understand its efficiency across the electromagnetic spectrum. As shown in Fig. 2B, this phosphor possesses a Φ of ≈80% when excited at 365 nm. The Φ improves as the excitation wavelength shifts to λ_{ex} = 400 nm, which is the highest Φ = 87%. Exciting the phosphor with blue light (λ_{ex} = 430 nm) causes a minor decrease with Φ = 83% while excitation at λ_{ex} = 450 nm leads to a Φ of ≈60%. The outstanding quantum yield for this phosphor is measured for samples directly out of the furnace and could easily be improved with further optimization and post-synthesis processing; nevertheless, the Φ allows this phosphor to be a viable green component in devices employing LED chips emitting between 365 nm and 430 nm.

The final test necessary for any phosphor prior to device consideration is the temperature dependent photoluminescence. LED-based lights operates at temperatures up to 150°C (423 K), and the effect of the elevated temperature on luminescence is significant. Evaluating the emission of NBBO:Eu_{Na} from 300 K to 700 K under λ_{ex} = 430 nm (Fig. 3A and 3B) shows an anomalous response where the relative integrated intensity continuously increases with a 30% increase in the emission intensity compared to the 300 K emission intensity before finally entering the quenching regime above 650 K. The peak intensity increases by 10% at 500 K, and then starts decreasing. The raw spectra at different temperature are plotted in Fig. S4. The origin of this surprising behavior is attributed to defects in the crystal structure resulting from the aliovalent substitution of Eu^{2+} for Na^{+}. This is supported by the emission intensity finally decreasing above 500 K as the electrons trapped in the defects are entirely released into the conduction band, and the emission is quenched. Unfortunately, all synthetic attempts to minimize the number of defects (e.g., annealing)

resulted in a loss the green emission. Additional research is required to understand the relationship between defects and the optical properties of this phosphor. Nevertheless, analyzing the emission color as a function of temperature shows a minimal shift in the color coordinates, as demonstrated on the 1931 CIE diagram in Fig. 3C. These excellent initial temperature dependent measurements further suggest this phosphor may be of industrial interest.

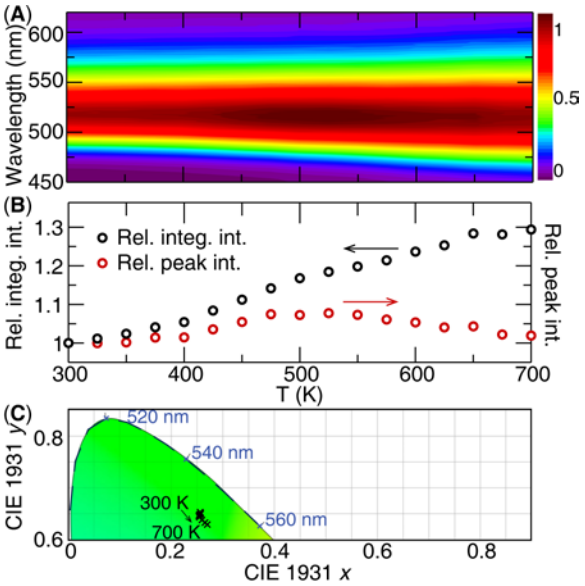

Fig. 3. Temperature dependent emission results. (**A**) Contour plot of the normalized emission spectra excited at 430 nm as a function of temperature. (**B**) The relative integrated intensity of the emission spectra (rel. integ. int.) and the relative intensity of the emission peak (rel. peak int.) as a function of temperature. (**C**) CIE coordinates of the emission color at 300 K, 400 K, 500 K, 600 K, and 700 K.

The narrow emission peak, bright green color, high efficiency, and thermal behavior of NBBO:Eu_{Na} demonstrates this phosphor might be worth considering further for LED-based lighting or display applications. This is reinforced by plotting the room temperature color coordinates of NBBO:Eu_{Na} alongside the industry-standard green phosphors β-SiAlON:Eu^{2+} and Ba_2SiO_4:Eu^{2+} on a 1931 CIE diagram (Fig. 4). Ba_2SiO_4:Eu^{2+} is on the very left of the color space owing to its broad, shorter emission wavelength, which gives its emission a blue hint that diminishes the color purity. In contrast, β-SiAlON:Eu^{2+} emits an almost monochromatic light but with a slight yellow shift. It also requires harsh synthetic conditions to prepare, which increases the phosphors market price driving up the consumer cost of any light bulbs or displays that use β-SiAlON:Eu^{2+}. These phosphors both lie outside the National Television System Committee (NTSC) color triangle, which makes them off the standard and decreases the color quality in a real display application. NBBO:Eu_{Na} is located in between Ba_2SiO_4:Eu^{2+} and β-SiAlON:Eu^{2+} in the color space, which moves this new phosphor's emission color closer to the green corner of the NTSC triangle providing potential improvements to color quality if this material was used in display applications. To ascertain the available color gamut covered if NBBO:Eu_{Na} were used in a device, the CIE coordinates were calculated in combination with a blue-emitting 430 nm LED and red-emitting K_2SiF_6:Mn^{4+}. Comparing the area of the resulting triangle created by connecting the coordinates for the LED–NBBO:Eu_{Na}–K_2SiF_6:Mn^{4+} system with the triangle created by LED–β-SiAlON:Eu^{2+}–K_2SiF_6:Mn^{4+} and the LED–Ba_2SiO_4:Eu^{2+}–K_2SiF_6:Mn^{4+} shows that using

NBBO:Eu_{Na} broadens the color gamut by 7% compared to these other phosphor systems. Further, NBBO:Eu_{Na} based triangle has an area that overlaps with 80% of the NTSC area, which is larger than a device using β-SiAlON:Eu^{2+} (69% of NTSC area) and Ba_2SiO_4:Eu^{2+} (66% of NTSC area) by permitting more color in the green wavelength region.

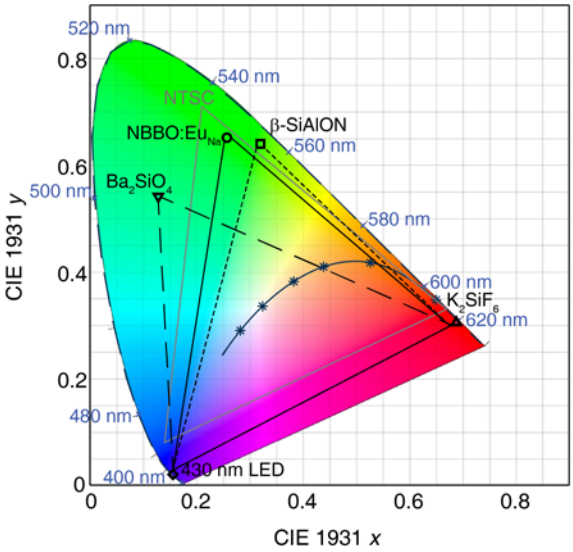

Fig. 4. Room temperature CIE coordinates. $(Na_{0.97}Eu_{0.03})BaB_9O_{15}$ excited at 430 nm (circle), Ba_2SiO_4:Eu^{2+} (down-triangle), β-SiAlON:Eu^{2+} (square), K_2SiF_6:Mn^{4+} (up-triangle), and 430 nm LED (diamond). Plotted in gray is the NTSC color space.

Conclusions

In summary, a highly-efficient narrow-band green-emitting phosphor, $(Na_{0.97}Eu_{0.03})BaB_9O_{15}$ was successfully synthesized by controlling the chemistry to drive the substitution of Eu^{2+} onto the smaller, less favorable [NaO_6] substitution site. The resulting phosphor has a high efficiency that makes it competitive with commercial phosphors. Indeed, the phosphor not only shows a $\Phi > 80\%$ using a blue or near-UV LED as the excitation source but it is also thermally robust and has a fast emission lifetime. This combination of optical properties along with its ease of synthesis suggests this bright green phosphor has outstanding potential in the general white lighting as well as the display lighting space. The development of this extraordinary phosphor was achieved by controlling preferential substitution, which has not yet been demonstrated in phosphor field before. These results undoubtedly provide a new approach for researchers to design new narrow-band phosphors and explore new classes of luminescent materials by controlling rare-earth substitution.

Materials and Methods

$(Na_{0.97}Eu_{0.03})BaB_9O_{15}$ and $Na(BaEu_{0.03})B_9O_{15}$ were prepared via solid-state reactions starting from $NaHCO_3$ (EM science, 99.7%), $BaCO_3$ (Johnson Matthey, 98%), H_3BO_3 (Sigma-Aldrich, 99.999%), and Eu_2O_3 (Materion Advanced Chemicals, 99.9%). The starting materials were loaded in the requisite stoichiometric ratios, thoroughly ground using an agate mortar and pestle, and subsequently sintered at 600 °C for 2 h in air to decompose the reagents and initiate the reaction. The samples were then ground and heated at 725 °C for 30 h for $(Na_{0.97}Eu_{0.03})BaB_9O_{15}$ and 780 °C for 30 h for $Na(Ba_{0.97}Eu_{0.03})B_9O_{15}$ using a fused silica tube furnace under a weak reducing

atmosphere (5% H_2/95% N_2) with heating and cooling ramps of 3 °C min^{-1}. Powder synchrotron X-ray diffraction data were collected at 295 K with a calibrated wavelength of 0.412824 Å (beamline 11-BM, Advanced Photon Source, Argonne National Laboratory).[23] The crystal lattice parameters were obtained from refinements based on the Rietveld method using the GSAS package with a shifted Chebyshev function employed to describe the background and a pseudo-Voigt function for determining peak shape.[30,31]

Photoluminescent spectra were recorded on a Horiba Fluoromax-4 fluorescence spectrophotometer with a 75 W xenon arc lamp with temperature controlled by a Janis liquid nitrogen cryostat (VPF-100). The sample was mixed into silicone resin (GE Silicones, RTV615) and deposited on a quartz substrate (Chemglass). The micrograph was taken with an Olympus IX73 optical microscope. The luminescence lifetime decay measurements were collected using a Horiba DeltaFlex Lifetime System equipped with a NanoLED N-390 nm LED (λ_{ex} = 392 nm) and a 450 nm long-pass filter. A total measurement length of 13 μs was employed using a repetition rate of 50 kHz and a delay of 10 ns. The absolute internal quantum yield was determined by placing the sample inside a Spectralon-coated integrating sphere (150 mm diameter, Labsphere) and exciting by n-UV through blue light of different wavelengths.[32]

Acknowledgments

General: This work used the resources available through the 11-BM beamline at the Advanced Photon Source, an Office of Science User Facility operated for the U.S. Department of Energy (DOE) Office of Science by Argonne National Laboratory, under Contract No. DE-AC02-06CH11357. **Funding:** The authors thank the National Science Foundation (DMR 18-47701 and CER 19-11311) as well as the R.A. Welch Foundation (E-1981) for supporting this work. **Author contributions:** Y.Z. and J.B. designed the research and wrote the paper. Y.Z. and J.Z. performed the research and analyzed the results. J.B. supervised the research. **Competing interests:** The authors declare no competing interests. **Data materials and availability:** All data needed to evaluate the conclusions in the paper are present in the paper and/or the Supplementary Materials. Additional data related to this paper may be requested from the authors.

References

(1) Pust, P.; Schmidt, P. J.; Schnick, W. A Revolution in Lighting. *Nat. Mater.* **2015**, *14* (5), 454–458.

(2) George, N. C.; Denault, K. A.; Seshadri, R. Phosphors for Solid-State White Lighting. *Annu. Rev. Mater. Res.* **2013**, *43* (1), 481–501.

(3) Liao, H.; Zhao, M.; Molokeev, M. S.; Liu, Q.; Xia, Z. Learning from a Mineral Structure toward an Ultra-Narrow-Band Blue-Emitting Silicate Phosphor $RbNa_3(Li_3SiO_4)_4:Eu^{2+}$. *Angew. Chemie* **2018**, *130* (36), 11902–11905.

(4) Pust, P.; Weiler, V.; Hecht, C.; Tücks, A.; Wochnik, A. S.; Henß, A.-K.; Wiechert, D.; Scheu, C.; Schmidt, P. J.; Schnick, W. Narrow-Band Red-Emitting $Sr[LiAl_3N_4]:Eu^{2+}$ as a next-Generation LED-Phosphor Material. *Nat. Mater.* **2014**, *13* (9), 891–896.

(5) Strobel, P.; Maak, C.; Weiler, V.; Schmidt, P. J.; Schnick, W. Ultra-Narrow-Band Blue-Emitting Oxoberyllates $AELi_2[Be_4O_6]:Eu^{2+}$ (AE=Sr,Ba) Paving the Way to Efficient RGB Pc-LEDs. *Angew. Chemie Int. Ed.* **2018**, *57* (28), 8739–8743.

(6) Li, S.; Wang, L.; Tang, D.; Cho, Y.; Liu, X.; Zhou, X.; Lu, L.; Zhang, L.; Takeda, T.; Hirosaki, N.; et al. Achieving High Quantum Efficiency Narrow-Band β-SiAlON:Eu^{2+} Phosphors for High-Brightness LCD Backlights by Reducing the Eu^{3+} Luminescence Killer. *Chem. Mater.* **2018**, *30*, 494–505.

(7) Huang, L.; Zhu, Y.; Zhang, X.; Zou, R.; Pan, F.; Wang, J.; Wu, M. HF-Free Hydrothermal Route for Synthesis of Highly Efficient Narrow-Band Red Emitting Phosphor $K_2Si_{1-x}F_6$:XMn^{4+} for Warm White Light-Emitting Diodes. *Chem. Mater.* **2016**, *28*, 1495–1502.

(8) Kim, Y. H.; Arunkumar, P.; Kim, B. Y.; Unithrattil, S.; Kim, E.; Moon, S.-H.; Hyun, J. Y.; Kim, K. H.; Lee, D.; Lee, J.-S.; et al. A Zero-Thermal-Quenching Phosphor. *Nat. Mater.* **2017**, *16* (5), 543–550.

(9) Qiao, J.; Ning, L.; Molokeev, M. S.; Chuang, Y.; Zhang, Q.; Poeppelmeier, K. R.; Xia, Z. Site-Selective Occupancy of Eu^{2+} Toward Blue-Light-Excited Red Emission in a $Rb_3YSi_2O_7$:Eu Phosphor. *Angew. Chemie* **2019**, *131* (33), 11654–11650.

(10) Wagatha, P.; Weiler, V.; Schmidt, P. J.; Schnick, W. Tailoring Emission Characteristics: Narrow-Band Red Luminescence from SLA to CaBa[Li 2 Al 6 N 8]:Eu 2+. *Chem. Mater.* **2018**, *30*, 7885–7891.

(11) Duke, A. C.; Hariyani, S.; Brgoch, J. $Ba_3Y_2B_6O_{15}$:Ce^{3+}: A High Symmetry, Narrow-Emitting Blue Phosphor for Wide-Gamut White Lighting. *Chem. Mater.* **2018**, *30*, 2668–2675.

(12) Yoshimura, K.; Fukunaga, H.; Izumi, M.; Masuda, M.; Uemura, T.; Takahashi, K.; Xie, R.-J.; Hirosaki, N. White LEDs Using the Sharp β-Sialon: Eu Phosphor and Mn-Doped Red Phosphor for Wide-Color Gamut Display Applications. *J. Soc. Inf. Disp.* **2016**, *24* (7), 449–453.

(13) Streit, H.; Kramer, J.; Suta, M.; Wickleder, C.; Streit, H. C.; Kramer, J.; Suta, M.; Wickleder, C. Red, Green, and Blue Photoluminescence of Ba_2SiO_4:M (M = Eu^{3+}, Eu^{2+}, Sr^{2+}) Nanophosphors. *Materials* **2013**, *6* (8), 3079–3093.

(14) Peters, T. E.; Baglio, J. A. Luminescence and Structural Properties of Thiogallate Phosphors Ce^{+3} and Eu^{+2}-Activated Phosphors. Part L. *J. Electrochem. Soc.* **1972**, *119*, 230–236.

(15) Zhao, M.; Liao, H.; Ning, L.; Zhang, Q.; Liu, Q.; Xia, Z. Next-Generation Narrow-Band Green-Emitting $RbLi(Li_3SiO_4)_2$:Eu^{2+} Phosphor for Backlight Display Application. *Adv. Mater.* **2018**, *30* (38), 1802489.

(16) Jang, E.; Jun, S.; Jang, H.; Lim, J.; Kim, B.; Kim, Y. White-Light-Emitting Diodes with Quantum Dot Color Converters for Display Backlights. *Adv. Mater.* **2010**, *22* (28), 3076–3080.

(17) Song, J.; Li, J.; Li, X.; Xu, L.; Dong, Y.; Zeng, H. Quantum Dot Light-Emitting Diodes Based on Inorganic Perovskite Cesium Lead Halides ($CsPbX_3$). *Adv. Mater.* **2015**, *27* (44), 7162–7167.

(18) Verma, S.; Verma, K.; Kumar, D.; Chaudhary, B.; Som, S.; Sharma, V.; Kumar, V.; Swart,

H. C. Recent Advances in Rare Earth Doped Alkali-Alkaline Earth Borates for Solid State Lighting Applications. *Phys. B Condens. Matter* **2018**, *535*, 106–113.

(19) Yu, R.; Zhong, S.; Xue, N.; Li, H.; Ma, H. Synthesis, Structure, and Peculiar Green Emission of $NaBaBO_3:Ce^{3+}$ Phosphors. *Dalt. Trans.* **2014**, *43* (28), 10969–10976.

(20) Zhong, J.; Zhao, W.; Zhuo, Y.; Yan, C.; Wen, J.; Brgoch, J. Understanding the Blue-Emitting Orthoborate Phosphor $NaBaBO_3:Ce^{3+}$ through Experiment and Computation. *J. Mater. Chem. C* **2019**, *7* (3), 654–662.

(21) Zhuo, Y.; Mansouri Tehrani, A.; Oliynyk, A. O.; Duke, A. C.; Brgoch, J. Identifying an Efficient, Thermally Robust Inorganic Phosphor Host via Machine Learning. *Nat. Commun.* **2018**, *9* (1), 4377.

(22) Penin, N.; Seguin, L.; Touboul, M.; Nowogrocki, G. Synthesis and Crystal Structure of Three $MM'B_9O_{15}$ Borates (M=Ba, Sr and M′=Li; M=Ba and M′=Na). *Int. J. Inorg. Mater.* **2001**, *3* (7), 1015–1023.

(23) Lee, P. L.; Shu, D.; Ramanathan, M.; Preissner, C.; Wang, J.; Beno, M. A.; Von Dreele, R. B.; Ribaud, L.; Kurtz, C.; Antao, S. M.; et al. A Twelve-Analyzer Detector System for High-Resolution Powder Diffraction. *J. Synchrotron Radiat.* **2008**, *15* (5), 427–432.

(24) Shannon, R. D. Revised Effective Ionic Radii and Systematic Studies of Interatomie Distances in Halides and Chaleogenides. *Acta Cryst* **1976**, *A32*, 751–767.

(25) Sun, J.; Zhang, X.; Du, H. Combustion Synthesis and Luminescence Properties of Blue $NaBaPO_4:Eu^{2+}$ Phosphor. *J. Rare Earths* **2012**, *30* (2), 118–122.

(26) Lu, F.-C.; Bai, L.-J.; Yang, B.-Z.; Yang, Z.-P. Synthesis, Structure and Photoluminescence of $BaAl_2Si_2O_8:Eu^{2+}$ Blue-Emitting Phosphors. *ECS J. Solid State Sci. Technol.* **2013**, *2* (11), R254–R257.

(27) Wang, Y.; Xu, X.; Yin, L.; Hao, L. High Thermal Stability and Photoluminescence of Si–N-Codoped $BaMgAl_{10}O_{17}:Eu^{2+}$ Phosphors. *J. Am. Ceram. Soc.* **2010**, *93* (6), 1534–1536.

(28) Hume-Rothery, W.; Powell, H. M. On the Theory of Super-Lattice Structures in Alloys. *Zeitschrift für Krist. - Cryst. Mater.* **1935**, *91* (1–6), 23–47.

(29) Wako, A. H.; Dejene, F. B.; Swart, H. C. Effect of Ga^{3+} and Gd^{3+} Ions Substitution on the Structural and Optical Properties of Ce^{3+} -Doped Yttrium Aluminium Garnet Phosphor Nanopowders. *Luminescence* **2016**, *31* (7), 1313–1320.

(30) Larson, A. C.; Von Dreele, R. B. *General Structure Analysis System (GSAS)*; Los Alamos, New Mexico, 1987.

(31) Toby, B. H. EXPGUI, A Graphical User Interface for GSAS. *J. Appl. Crystallogr.* **2001**, *34* (2), 210–213.

(32) Leyre, S.; Coutino-Gonzalez, E.; Joos, J. J.; Ryckaert, J.; Meuret, Y.; Poelman, D.; Smet, P. F.; Durinck, G.; Hofkens, J.; Deconinck, G.; et al. Absolute Determination of Photoluminescence Quantum Efficiency Using an Integrating Sphere Setup. *Rev. Sci. Instrum.* **2014**, *85* (12), 123115.

Supplementary Materials

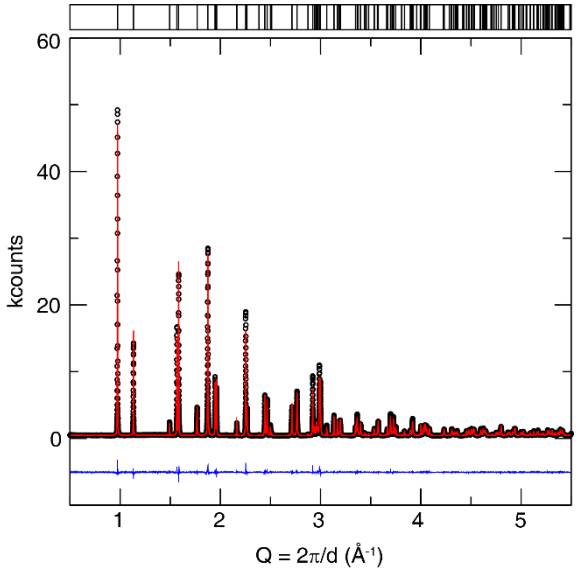

Fig. S1. Rietveld refinement of $Na(Ba_{0.97}Eu_{0.03})B_9O_{15}$ synchrotron X-ray powder diffraction data. The observed data are colored black, the refinement is colored red, and the difference is colored blue.

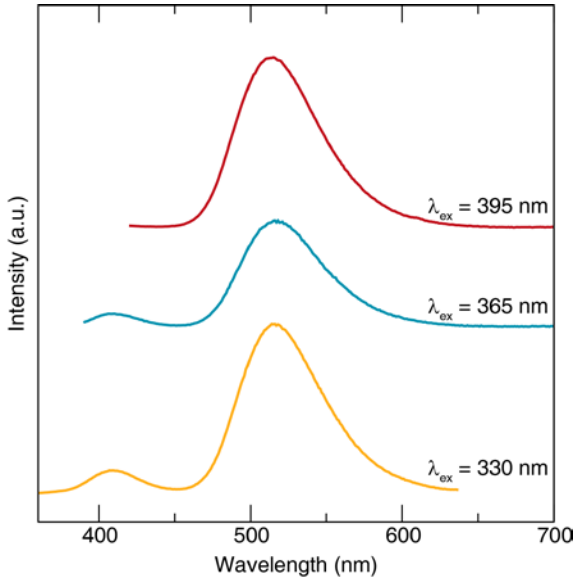

Fig. S2. Room temperature emission spectra at different excitation wavelength.

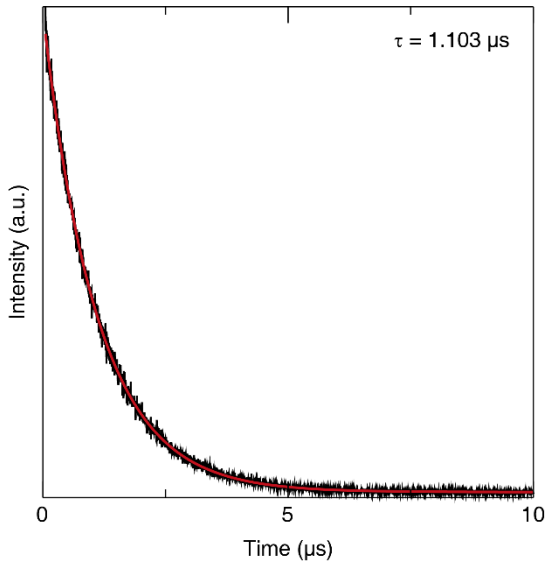

Fig. S3. Luminescence lifetime curve of $(Na_{0.97}Eu_{0.03})BaB_9O_{15}$. The lifeime (τ) is obtained by fitting the data with a single exponential function which is shown in red.

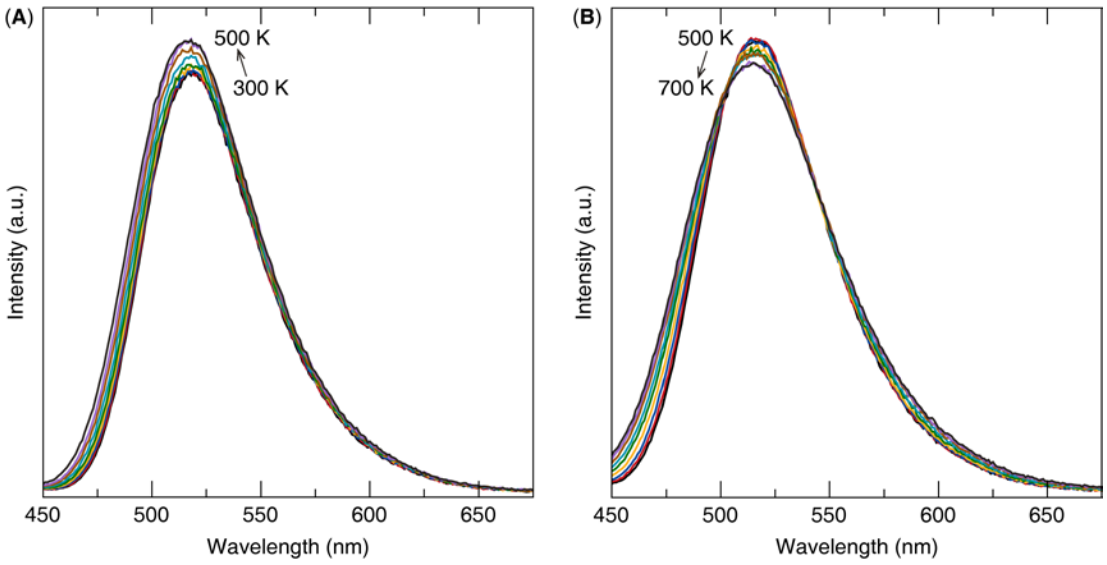

Fig. S4: Emission spectra excited at 430 nm under different temperatures. (**A**) 300 K – 500 K and (**B**) 500 K – 700 K.

Table S1. Atomic coordinates and isotropic displacement parameters of $Na(Ba_{0.97}Eu_{0.03})B_9O_{15}$. Results are determined by Rietveld refinement of 11-BM synchrotron X-ray powder diffraction.

Atom	Wyck.	*x*	*y*	*z*	U_{iso} (Å^2)
Ba(1)	6a	0	0	0	0.0104(7)
Na(1)	6a	0	0	0.22131(5)	0.0104(2)
B(1)	18b	0.39040(6)	0.26606(6)	0.05509(7)	0.0047(8)
B(2)	18b	0.45007(9)	0.39491(4)	0.17021(6)	0.0067(7)
B(3)	18b	0.2275(2)	0.3323(4)	0.11349(9)	0.0049(4)
O(1)	18b	0.47948(6)	0.32682(6)	0.11421(8)	0.0063(5)
O(2)	18b	0.25361(3)	0.24268(1)	0.05985(8)	0.0009(9)
O(3)	18b	0.20186(5)	0.43162(3)	0.06750(4)	0.0020(8)
O(4)	18b	0.34201(2)	0.41441(9)	0.16377(4)	0.0018(8)
O(5)	18b	0.10440(6)	0.23191(5)	0.15901(4)	0.0027(1)

Table S2. Atomic coordinates and isotropic displacement parameters of $(Na_{0.97}Eu_{0.03})BaB_9O_{15}$. Results are determined by Rietveld refinement of 11-BM synchrotron X-ray powder diffraction.

Atom	Wyck.	*x*	*y*	*z*	U_{iso} (Å^2)
Ba(1)	6a	0	0	0	0.0134(6)
Na(1)	6a	0	0	0.22127(2)	0.0133(4)
B(1)	18b	0.39052(9)	0.2660(8)	0.05256(3)	0.0065(8)
B(2)	18b	0.45251(4)	0.39417(7)	0.16923(6)	0.0086(4)
B(3)	18b	0.22328(9)	0.33062(3)	0.11496(9)	0.0080(3)
O(1)	18b	0.47905(6)	0.32843(2)	0.11344(4)	0.0085(5)
O(2)	18b	0.25507(6)	0.24405(5)	0.05803(3)	0.0054(7)
O(3)	18b	0.20434(3)	0.43031(2)	0.0659(7)	0.0057(4)
O(4)	18b	0.34417(4)	0.41625(5)	0.16314(3)	0.0020(5)
O(5)	18b	0.10550(2)	0.23054(4)	0.15890(7)	0.0038(1)